Nuclear Science and Techniques (2026) 37:99
https://doi.org/10.1007/s41365-026-01922-5

Three-dimensional full-scale neutronics/thermal-hydraulics/mechanics coupling analysis-based structural assessment of helium-cooled ceramic breeder blanket for fusion reactor

Qiang Lian[1,2,3] · Kui Zhang[4] · Shan-Shan Bu[1,2] · Liang-Ming Pan[1,2] · Wen-Xi Tian[4] · Sui-Zheng Qiu[4] · Guang-Hui Su[4] · Xing-Hua Wu[5] · Xiao-Yu Wang[5]

Received: 9 August 2024 / Revised: 1 November 2024 / Accepted: 29 November 2024 / Published online: 24 March 2026

Abstract
To accelerate the development and utilization of fusion energy, the China Fusion Engineering Test Reactor (CFETR) has been proposed as a bridge between the International Thermonuclear Experimental Reactor and demonstration fusion reactors. The primary objective of the CFETR is to achieve fusion energy transformation and tritium self-sufficiency, which is realized through the function of the blanket. In this study, a neutronics/thermal-hydraulics/mechanics coupling method is developed and applied to a helium-cooled ceramic breeder (HCCB) blanket, which is one of the two blanket candidates for the CFETR. A three-dimensional full-scale model is utilized in the coupling analysis to obtain the distributions of the neutronic, thermal-hydraulic, and mechanical parameters. A structural assessment of the CFETR HCCB blanket is then conducted considering steady-state conditions and two transient scenarios. The results demonstrate that following optimization of the blanket structure, the maximum temperatures of the different components remain below the safety limit of the corresponding materials. The structural assessment indicates that the blanket maintains its structural integrity under steady-state conditions. However, immediately after an in-box loss-of-coolant accident, structural failure owing to stress concentration may occur. Additionally, in the early stage of a loss-of-flow accident, the stress at the joint point between the cooling plate and cap exceeds the allowable stress of the material, potentially leading to structural failure within 17 s if no protective response is implemented. These findings provide comprehensive insights into the performance and safety of the CFETR HCCB blanket design.

Keywords Structural assessment · Fusion blanket · Three-dimensional full-scale model · Coupling analysis · CFETR

1 Introduction

The blanket is a core component of fusion reactors for achieving energy self-sustainability and thermal–electric conversion [1, 2] and serves as a crucial functional carrier for the practical application of fusion energy. The main functions of the blanket in a fusion reactor include tritium breeding [3–5], energy transfer [6, 7], and radiation shielding [8,

This work was supported by the National Natural Science Foundation of China (Nos. 12405194 and 52276052), the National Key R&D Program of China (Nos. 2024YFE03230200 and 2022YFE03160002), and the Natural Science Foundation of Chongqing, China (No. CSTB2025NSCQ-GPX0761).

✉ Qiang Lian
lianq@cqu.edu.cn

1 Key Laboratory of Low-Grade Energy Utilization Technologies and Systems, Chongqing University, 400044 Chongqing, China

2 Department of Nuclear Engineering and Technology, Chongqing University, 400044 Chongqing, China

3 Postdoctoral Station of Materials Science and Engineering, Chongqing University, 400044 Chongqing, China

4 School of Nuclear Science and Technology, Xi'an Jiaotong University, 710049 Xi'an, China

5 Center for Fusion Science, Southwestern Institute of Physics, 610225 Chengdu, China

9]. The blanket operates in a complex environment and enduring high heat flux loads and neutron impacts [10, 11]. Both the functionality and safety requirements of the blanket require the material temperature limits, tritium production rate, and structural integrity to be satisfied [12]. Therefore, neutronics/thermal-hydraulics/mechanics coupled analysis should be performed during the blanket design phase to ensure that the blanket can fulfill its normal functions and operate safely.

The International Thermonuclear Experimental Reactor (ITER) was launched through worldwide collaborations. However, ITER is primarily focused on scientific research and does not include the net energy output. To further develop the fusion technology, many countries have proposed plans for the demonstration of fusion reactors. China also intends to develop its own fusion technology and has proposed the Chinese Fusion Engineering Test Reactor (CFETR) to verify the feasibility of fusion engineering goals [13]. The CFETR is primarily aimed at achieving energy output and tritium self-sufficiency. A helium-cooled ceramic breeder (HCCB) blanket was designed by the Southwestern Institute of Physics (SWIP) and extensive performance analyses were conducted [14–19]. As an inherited concept from the Chinese helium-cooled ceramic breeder test blanket module (CH HCCB TBM) for ITER [20], the HCCB blanket has great potential for application in CFETR [21].

Several studies have been conducted on multiphysics coupling analysis and structural assessment of fusion blankets. For instance, in the case of a CFETR helium-cooled solid blanket, an electromagnetic–thermal–mechanical coupling analysis was performed [22, 23]. The results revealed significant coupling effects during certain magnetic field transients. However, the structural design requirements could still be satisfied even under the main disruption events, with

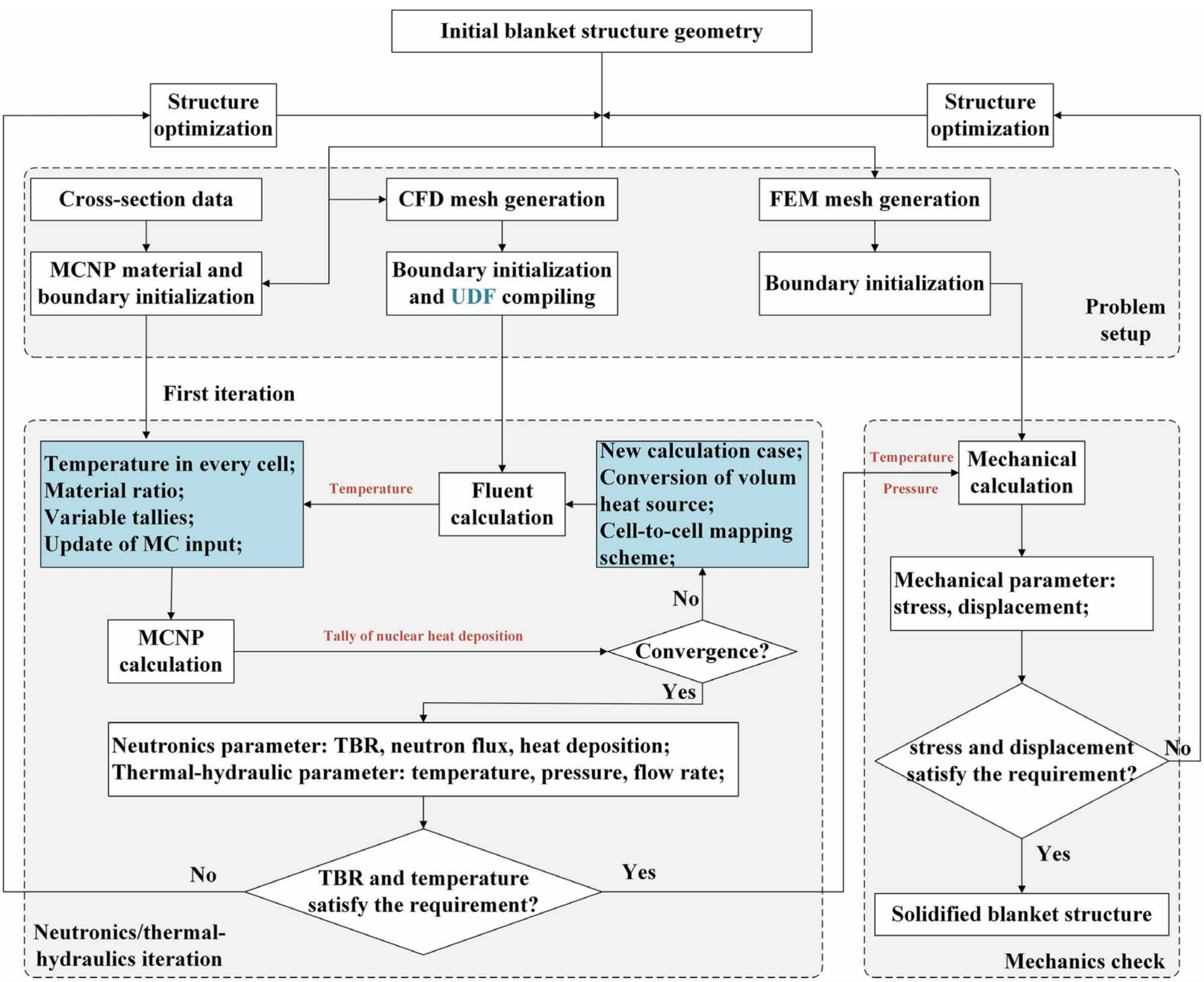

Fig. 1 (Color online) Coupling analysis procedure

stresses remaining within the allowable stress limit. The influence of the electromagnetic field on the blanket structure was also investigated under steady state and major plasma disruption events [24, 25]. A numerical study was conducted to investigate the multiphysics characteristics of the CFETR helium-cooled solid blanket by employing a neutronics/thermal-hydraulics/mechanics coupling analysis [26]. In this study, a slice-layer model was utilized to account for the repetitive structure along the poloidal direction. Parametric sensitivity analysis was performed to optimize the blanket structure. Structural failure occurred during an in-box loss-of-coolant accident (LOCA), in which the high-pressure helium coolant leaked into the blanket box. A neutronic-thermal-hydraulic–mechanic-coupled platform was developed specifically for the water-cooled ceramic breeder blanket of CFETR [27]. A comparison between two-dimensional (2D) and three-dimensional (3D) thermal analyses revealed that 3D coupling is essential. This is primarily because of the significant temperature difference, reaching 300 °C, as observed at the back of the blanket [27, 28]. In addition to the aforementioned studies, a neutronics/thermal-hydraulics/mechanics coupling analysis was conducted for the supercritical water-cooled ceramic blanket of CFETR [29]. The results of this analysis highlighted the need to incorporate an interlayer to withstand the thermal stress on the first wall. This suggests that the inclusion of an interlayer is crucial for ensuring the structural integrity and performance of the blanket. A study was conducted to analyze the structural performance of a helium-cooled pebble-bed blanket for a European demonstration (EU DEMO) fusion reactor [30]. This investigation focused on examining both the thermal and structural aspects of the blanket. Their findings indicated that the primary cause of damage to the blanket structure was the presence of high-temperature gradients. These temperature differences were identified as the critical factors contributing to the structural degradation of the blanket. A water-cooled lead–lithium blanket, another type of blanket proposed for the EU DEMO fusion reactor, was assessed in a separate study [31]. This assessment suggested that the attachment system should be revised to minimize displacement and reduce stress levels within the blanket.

In most of the aforementioned studies, the slice layer model was adopted because of the similarity and symmetry of the blanket structure along the poloidal direction

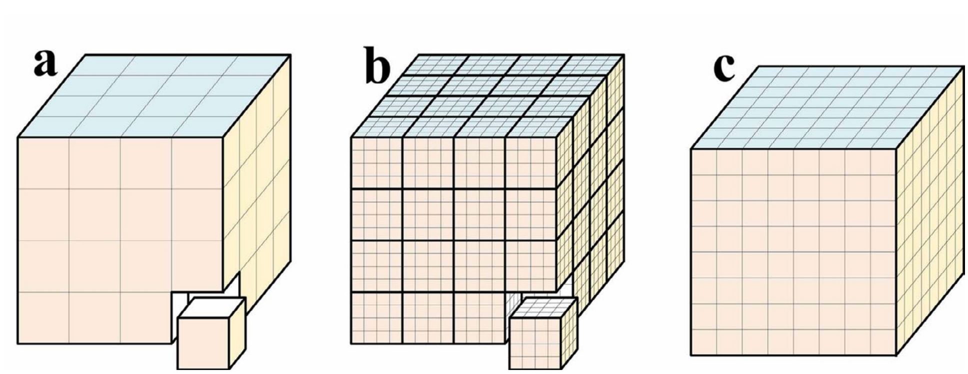

Fig. 2 (Color online) Data mapping scheme in coupling analysis: **a** Neutronics cell; **b** Thermal-hydraulic cell and mesh; and **c** Mechanical mesh

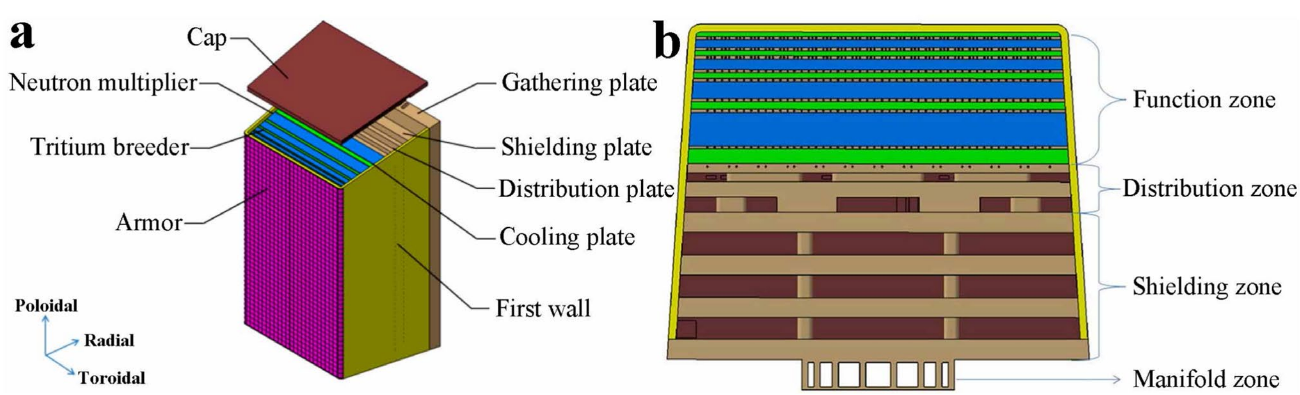

Fig. 3 (Color online) Structure design of CFETR HCCB TBB: **a** Overall view and **b** Poloidal cross-section

under the assumption of a uniform neutron distribution. However, such a simplification cannot be satisfied with the nonuniform neutron distribution imposed on the blanket during its operation. The blanket performance cannot be characterized using the slice layer model because of the interaction between adjacent zones along the poloidal direction. Therefore, considering the nonuniform boundary conditions [16, 32] and discrepancies between 2D and 3D models [27, 28], using a 3D blanket model for the structural design and performance analysis of the blanket is recommended. In this study, we aimed to develop and apply a neutronics/thermal-hydraulics/mechanics coupling method to a 3D full-scale model of the CFETR HCCB blanket. The material temperature requirement was considered in the optimization of the blanket structure through neutronics/thermal-hydraulics coupling analysis. Subsequently, a structural assessment of the optimized blanket was conducted via coupling analysis under steady-state conditions and two transient scenarios. The results obtained are presented and discussed based on the stress linearization method for different components in the optimized blanket. The comprehensive 3D full-scale coupling analysis and structural assessment results provide valuable guidance for the structural design of the CFETR HCCB blanket.

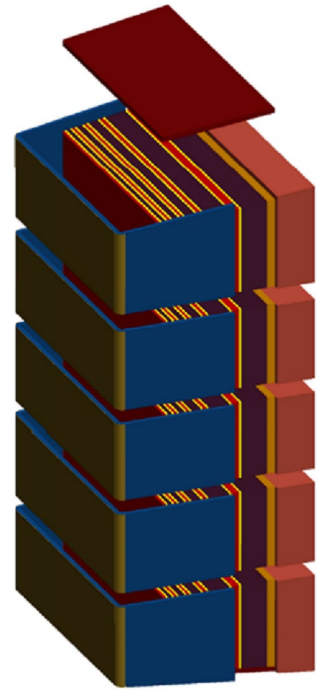

Fig. 4 (Color online) 3D full-scale neutronics model of CFETR HCCB blanket

2 Development of neutronics/thermal-hydraulics/mechanics coupling method

For the coupling analysis in this study, data mapping between different physics fields was achieved through neutronics, thermal-hydraulics, and mechanical calculations, which were performed using MCNP4C [33], Fluent [34], and ANSYS Mechanical [35]. To account for the distinct characteristics of each calculation process, a volume-weighted cell-to-cell mapping scheme was employed for the data transfer between MCNP4C and Fluent. This scheme ensures that data are accurately exchanged between the two software packages. Additionally, data transfer between fluent and mechanical was accomplished using the ANSYS Workbench platform, which provides seamless integration with the definition of a data transfer algorithm. The development and application of the coupling method, including data mapping procedures and the 3D models, are described in detail in this section. This ensures that the coupling analysis is performed effectively and efficiently, enabling accurate and reliable results.

2.1 Coupling approach

The neutronics/thermal-hydraulics/mechanics coupling analysis procedure is shown in Fig. 1. First, based on the design of the blanket structure, iterative calculations are performed for neutronics and thermal-hydraulics calculations. If the temperature of all the materials is within the required temperature range, then the pressure and temperature data are used in the mechanics calculations to determine the distribution of stress and deformation. Subsequently, a structural assessment is conducted to verify whether the structural requirements are met. During the coupling analysis, if any

Table 1 Design parameters for the blanket No. 3

Design item	Parameters
Overall geometry	1250 mm (toroidal frontal) × 1110 mm (radial) × 2110 mm (poloidal frontal)
FW	Direction: radial-toroidal-radial; Thickness: 25 mm (3/12/10)
	Channel cross-section: 19 mm × 12 mm; Pitch: 25 mm; Chamfer: 3 mm
Cap	Geometry: radial-toroidal trapezoid; Thickness: 25 mm (3/12/10)
Function zone	Geometry: square frustum box; Radial thickness: 565 mm
	Cooling plate direction: toroidal-poloidal; Thickness: 10 mm (2/6/2)

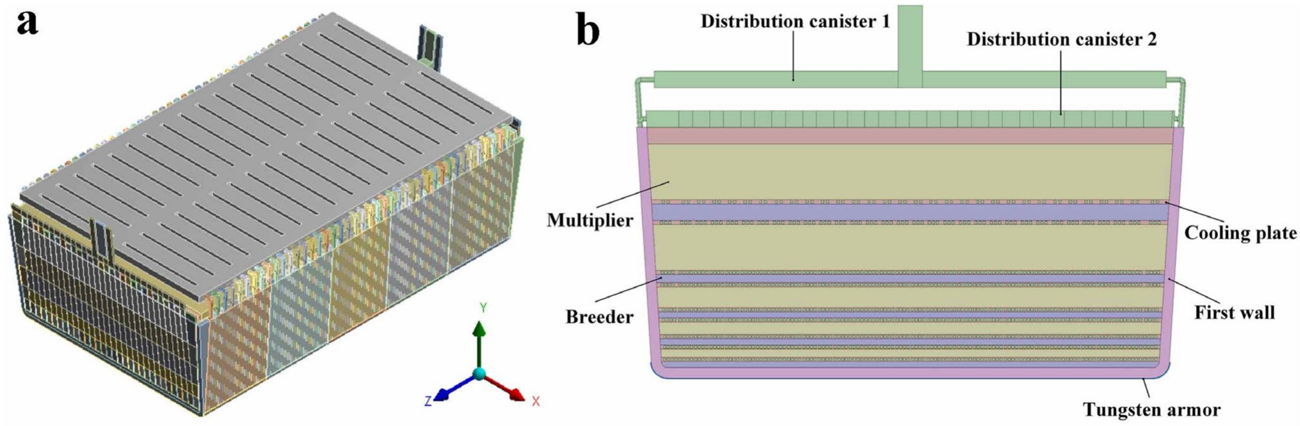

Fig. 5 (Color online) 3D full-scale thermal-hydraulic model of CFETR HCCB blanket: **a** Whole geometry model and **b** Poloidal cross-section

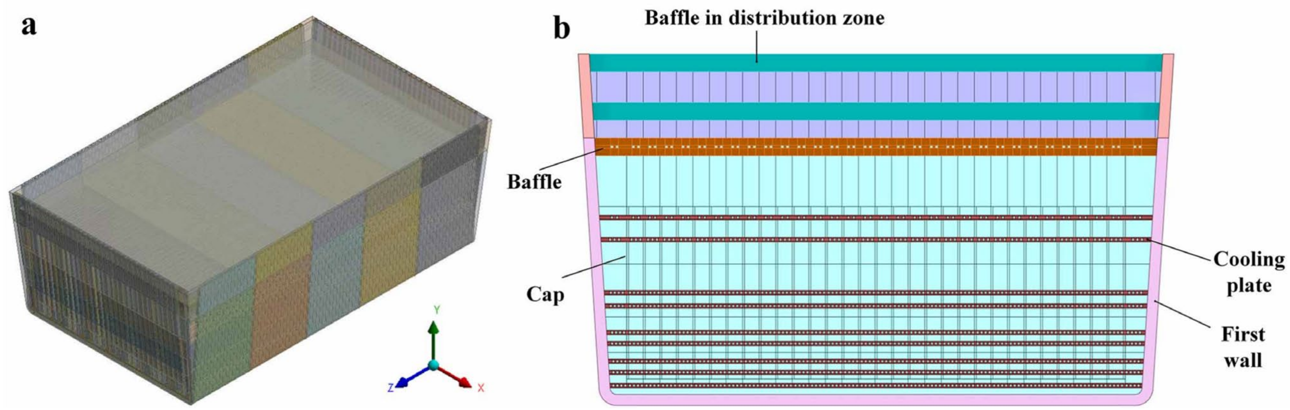

Fig. 6 (Color online) 3D full-scale mechanical model of CFETR HCCB blanket: **a** Whole geometry model and **b** Poloidal cross-section

Table 2 Comparison of heat source during neutronics/thermal-hydraulics coupling analysis

Component	Q_{in} (W·m^{-3})	Q_{ex} (MeV·m^{-3})	Q_{tr} (W·m^{-3})	Component	Q_{in} (W·m^{-3})	Q_{ex} (MeV·m^{-3})	Q_{tr} (W·m^{-3})
Breeder 1	12.90	6196.41	12.90	FW	4.20	2018.46	4.20
Breeder 2	8.14	3908.26	8.14	CP 1	2.98	1429.76	2.98
Breeder 3	4.73	2269.53	4.73	CP 21	2.37	1138.68	2.37
Breeder 4	3.22	1545.87	3.22	CP 22	2.15	1031.82	2.15
Breeder 5	1.56	746.74	1.56	CP 31	1.90	913.90	1.90
Multiplier 1	0.89	429.63	0.89	CP 32	1.87	897.43	1.87
Multiplier 2	0.51	245.34	0.51	CP 41	1.63	784.42	1.63
Multiplier 3	0.41	195.28	0.41	CP 42	1.36	654.71	1.36
Multiplier 4	0.31	149.63	0.31	CP 51	1.13	540.65	1.13
Multiplier 5	0.19	90.99	0.19	CP 52	0.71	342.69	0.71

factor fails to satisfy the safety requirements, the blanket structure must be optimized, and the coupling analysis must be performed again. This iterative process ensures that the neutronics, thermal-hydraulics, and mechanical aspects are properly integrated and evaluated, allowing for the optimization of the blanket structure and ensuring its compliance with safety standards.

A user-defined function (UDF) is compiled within Fluent to enable neutronics/thermal-hydraulics coupling analysis [36]. The UDF facilitates automatic data transfer between neutronics and thermal-hydraulic calculations through cell-to-cell mapping. As depicted in Fig. 2 (a) and (b), the geometric cells in MCNP have a one-to-one correspondence with the calculation domain in Fluent. Meshes are generated in each domain for thermal-hydraulic analysis. The nuclear heat deposition obtained from the neutronics calculations is transferred to all meshes as an internal heat source in the respective thermal-hydraulic domain. For the iterative calculation, the volume-averaged temperature of all meshes in the thermal-hydraulic domain is transferred back to the corresponding neutronics cell. Subsequently, the nuclear cross-sectional data are adjusted to account for the temperature effect during the neutronics calculations. The entire neutronics/thermal-hydraulics coupling algorithm, including data transfer, parameter output, MCNP input update, and extraction of heat deposition from MCNP output, is embedded in the UDF, which is described in detail in our previous work [37].

Once the iterative calculation for the neutronics/thermal-hydraulics coupling analysis converged, the temperature and pressure data are transferred to the mechanical calculation for a mechanics check and structural assessment. Although the thermal-hydraulic mesh differs significantly from the mechanical mesh, as shown in Fig. 2 (b) and (c), data transfer between the thermal-hydraulics and mechanics calculations can still be achieved within the Workbench platform through point-to-point mapping. The received data were calculated through interpolation using the original data from neighboring points. Notably, in the neutronics/thermal-hydraulics coupling analysis, the thermal-hydraulic geometry is partitioned for cell-to-cell data mapping. Conversely, for mechanical calculations, geometry partitioning is not required. Therefore, after establishing an appropriate many-to-one cell geometry mapping within Workbench, the temperature and pressure data can be transferred to the mechanics calculations.

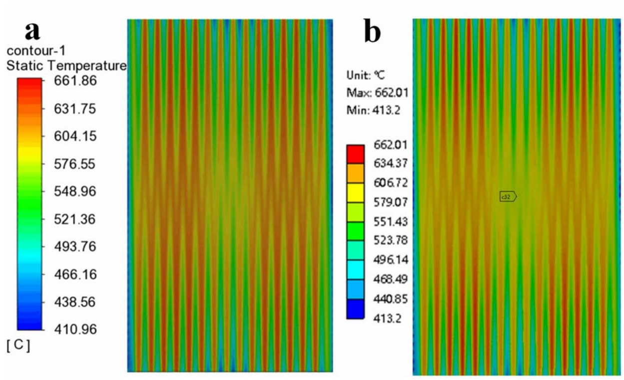

Fig. 7 (Color online) Comparison of CP32 temperature in thermal-hydraulics/mechanics coupling analysis: **a** output parameter and **b** received parameter

2.2 Model development for coupling analysis

A typical HCCB blanket for CFETR is illustrated in Fig. 3. It comprises four radially arranged zones: function, distribution, shielding, and manifold. These zones are integrated within the blanket box, which consisted of the first wall (FW), caps, and a gathering plate. To protect the blanket from radiation heat flux and high-energy neutrons produced by the ultra-high-temperature plasma, a 2-mm-thick tungsten layer is coated on the frontal side of the FW. The primary functions of the blanket include tritium breeding and energy conversion, which are primarily achieved in the functional zone. Tritium breeding occurs through a nuclear reaction between neutrons and the breeder material, lithium orthosilicate (Li_4SiO_4) [38]. To enhance the breeding capability, beryllium neutron multipliers are incorporated into the blanket to provide additional neutrons for tritium breeding. The breeders and multipliers separated by cooling plates (CPs) are arranged in layers along the radial direction.

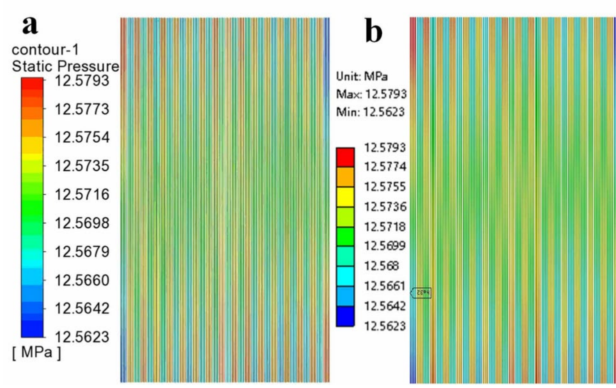

Fig. 8 (Color online) Comparison of CP32 pressure in thermal-hydraulics/mechanics coupling analysis: **a** output parameter and **b** received parameter

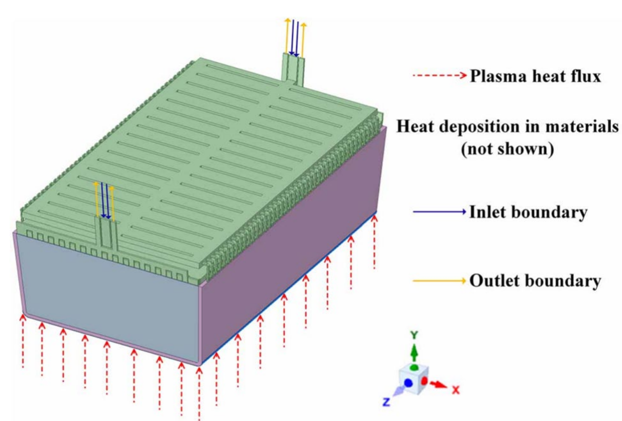

Fig. 9 (Color online) Boundary condition for thermal-hydraulic analysis

The structural components within the blanket, which bear mechanical stress as a skeleton structure, are composed of oxide dispersion-strengthened reduced activation ferritic/martensitic (ODS RAFM) steel. The dispersed oxide allows the temperature limit of RAFM steel to increase from 550 °C to 650 °C, which contributes to a larger temperature window for coolant [15, 18, 39]. The helium coolant flows successively through the FW, caps, and CPs to extract the plasma heat flux and nuclear heat deposition from the blanket. The designed working conditions involve a pressure of 12 MPa and temperatures of 300 °C/600 °C. The main geometrical parameters of the typical blanket are provided in Table 1.

Figure 4 illustrates a 3D full-scale neutronics model of the CFETR HCCB blanket. The neutron wall loading (NWL) of the FW can be obtained by neutronics analysis of the entire Tokamak device [40]. Then, the corresponding NWL can be used for the neutronics simulation of a particular blanket [14, 15, 20, 23]. Owing to the nonuniform distribution of NWL [16], the neutronics model is divided into five poloidal parts. In addition, the model is partitioned in the radial and toroidal directions to account for the gradients of the major parameters, particularly in the corner region of the blanket. The 3D full-scale neutronics model is converted using CAD geometry [41, 42] to reduce the model error in the MC calculation. Figure 5 presents a 3D full-scale thermal-hydraulic model of the CFETR HCCB blanket. While the original geometry model for the thermal-hydraulic analysis is similar to that used in the neutronics analysis, certain simplifications are implemented to alleviate modeling complexities. In the distribution zone, for instance, only the liquid domain is modeled because this zone primarily serves the purpose of distributing and collecting helium coolant with minimal heat source contribution. The shielding and manifold zones are also excluded from the thermal-hydraulic analysis. The flow–heat transfer coupling is solely modeled in the functional zone of the blanket to investigate the temperature distribution within the blanket. Figure 6 depicts a 3D full-scale mechanical model of the CFETR HCCB blanket. The mechanical model focuses solely on the primary skeleton structure of the blanket, whereas other components that were not subjected to mechanical stress are omitted. Similar to the neutronics and thermal-hydraulics models, the mechanical model is divided into five poloidal parts to simplify the data transfer between the thermal-hydraulic and mechanical calculations, ensuring a coherent analysis approach.

2.3 Validation of the data transfer during coupling analysis

To ensure physical conservation during coupling analysis, the data transfer is validated by comparing the output parameter Φ_{ex} with the received parameter Φ_{in}. In the neutronics/thermal-hydraulics coupling analysis, the nuclear heat deposition is tallied in $MeV \cdot m^{-3}$ but converted into $W \cdot m^{-3}$ for consistency. Table 2 presents the received volumetric heat source Q_{in} in the thermal-hydraulic analysis, the output nuclear heat deposition Q_{ex} in neutronics analysis, and the converted volumetric heat source Q_{tr}. Because of the cell-to-cell data mapping method employed in the neutronics/thermal-hydraulics coupling analysis, the nuclear heat deposition obtained from the neutronics calculations is transferred to all the meshes

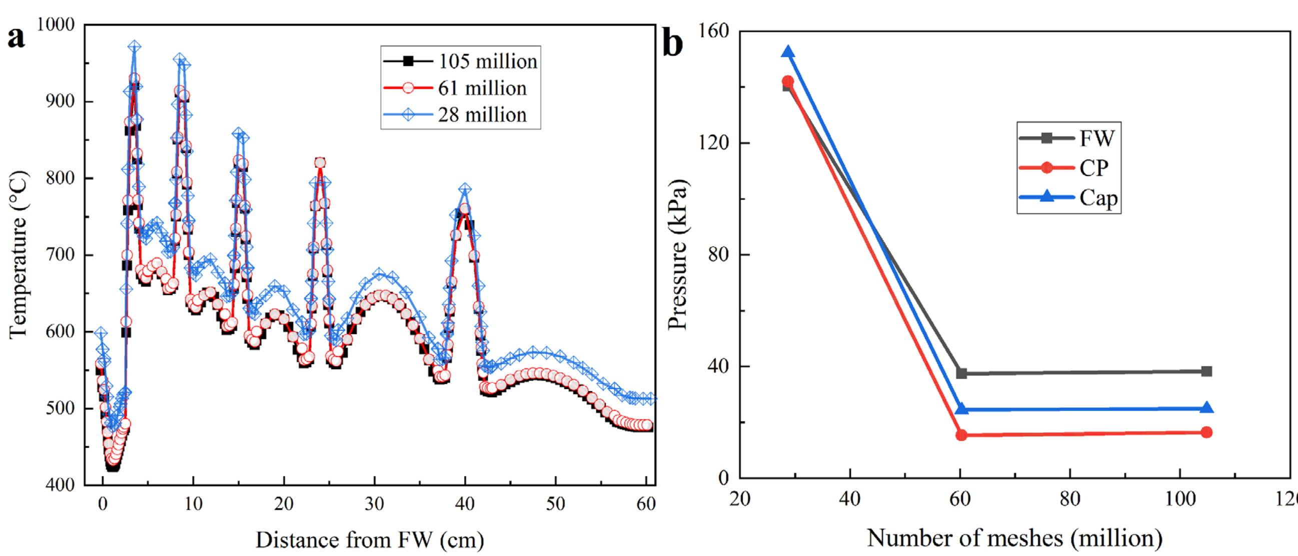

Fig. 10 (Color online) Mesh sensitivity analysis for thermal-hydraulics calculation: **a** Temperature distribution along the blanket centerline and **b** Pressure drop

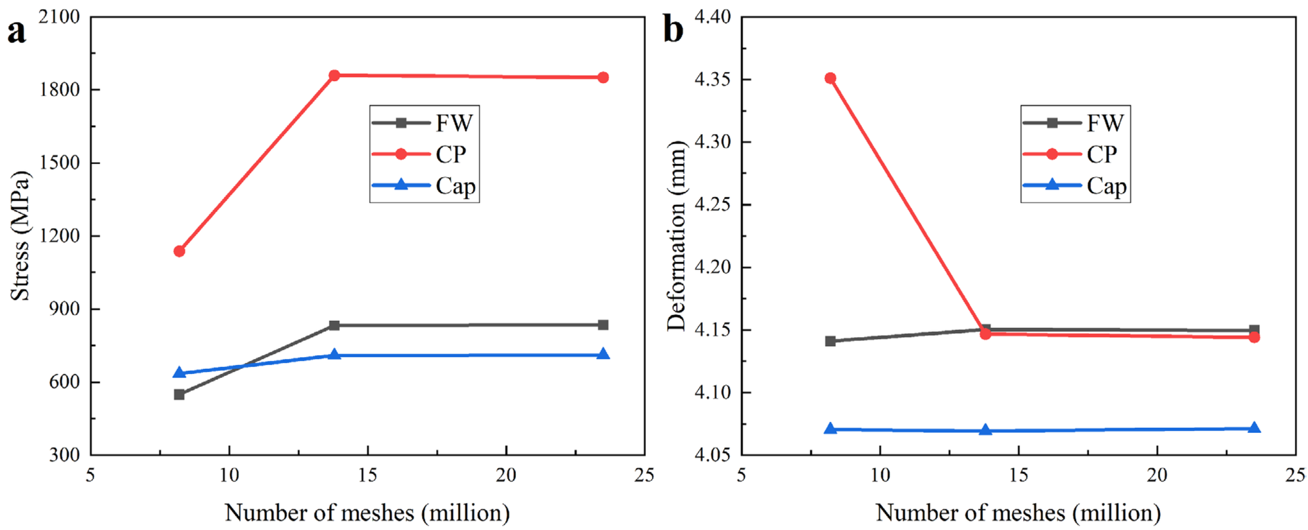

Fig. 11 (Color online) Mesh sensitivity analysis for mechanics calculation: **a** Maximum stress and **b** Maximum deformation

Table 3 Radial thickness before and after structure optimization

Component	Initial value (mm)	Final value (mm)	Component	Initial value (mm)	Final value (mm)
Breeder 1	15	8	Multiplier 1	20	15
Breeder 2	15	10	Multiplier 2	30	25
Breeder 3	15	12	Multiplier 3	50	40
Breeder 4	20	15	Multiplier 4	110	100
Breeder 5	40	40	Multiplier 5	135	185

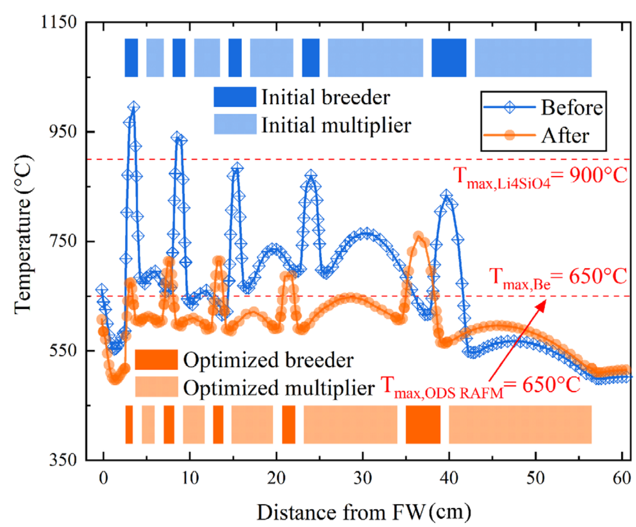

Fig. 12 (Color online) Temperature distribution along the blanket centerline before and after structure optimization

as the internal heat source in the corresponding thermal-hydraulic domain. Consequently, Q_{in} and Q_{tr} are equal for each component, ensuring energy conservation throughout the neutronics/thermal-hydraulics coupling analysis. In the thermal-hydraulics/mechanics coupling analysis, the temperature and pressure data are interpolated between the two meshes through adjacent point-to-point mapping. Comparisons between the output parameter Φ_{ex} in the thermal-hydraulic analysis and the received parameter Φ_{in} in the mechanics analysis of cooling plate CP32 are illustrated in Figs. 7 and 8. It can be observed that the distribution of the received parameter is nearly identical to that of the output parameter, with minimal differences. These discrepancies arise primarily from the variation in the mesh sizes between the two physical domains. However, the largest temperature difference remains below 3 °C, and the pressure difference remains below 100 Pa. Such small differences are acceptable to meet the accuracy requirements for data transfer. These results indicate that the interpolation method effectively transfers the temperature and pressure data between the thermal and hydraulic and mechanical calculations, ensuring the correctness and reliability of the data transfer process.

3 Performance analysis of CFETR HCCB blanket

3.1 Boundary condition

In the neutronics analysis, a neutron source with an energy of 14.1 MeV is located on the frontal surface of the FW [43]. The back surface is set as a transmitting boundary, whereas reflecting boundaries are applied to the other surfaces [44].

The nonuniform neutron distribution is also considered in accordance with our previous study [16]. The boundary conditions for the thermal-hydraulic analysis are illustrated in Fig. 9. Plasma heat flux is imposed on the frontal surface of the FW, whereas the remaining surfaces are considered adiabatic. The inlet and outlet boundaries are specified using velocity and pressure conditions, respectively. To accurately capture the high-speed helium flow in all channels, a reliable k-ϵ turbulence model is adopted, considering the sensitivity analysis of the helium heat transfer as referenced in [39]. Internal heat sources are incorporated into the meshes based on the results obtained from neutronics analysis. In the mechanical analysis, the pressure distribution on the channel surface is determined using the thermal–hydraulic analysis results. Similarly, the temperature distribution in the solid phase is considered. Gravity effects are considered for the entire blanket skeleton. In addition, a fixed constraint condition is applied to the back surface to restrict blanket displacement. These boundary conditions and constraints enable a comprehensive analysis of the neutronics, thermal-hydraulics, and mechanical aspects, providing an accurate representation of the behavior and performance of the CFETR HCCB blanket.

3.2 Mesh independence

The mesh independence analysis primarily focuses on thermal-hydraulics and mechanical calculations. The mesh generation method is first validated for basic models by comparison with experimental results, and the validation of the thermal–hydraulic calculation is described in detail in [39]. Subsequently, the experience is used for the mesh generation of the entire blanket module. In the mesh independence analysis of the thermal-hydraulic calculation, three different mesh systems were generated. These systems consisted of 105, 61, and 28 million meshes, respectively. Figure 10(a) shows the temperature distributions along the centerline of the blanket for the three mesh systems. It can be observed that the difference in the temperature distribution is minimal between the first and second mesh systems. However, for the third mesh system, a significant temperature difference of up to 60 °C is identified, indicating that this particular mesh system is not suitable for an accurate thermal–hydraulic analysis. Figure 10(b) shows the pressure drops in different channels for the three mesh systems. The pressure drop obtained using the third mesh system is excessively large, whereas the other two mesh systems yielded similar pressure drops for all components. Considering the influence of the mesh system on both the temperature distribution and pressure drop, a mesh system with 61 million meshes is the most appropriate for the subsequent thermal-hydraulics analysis.

In the mesh independence analysis of the mechanical calculations, three different mesh systems are generated with varying numbers of meshes: 23.5 million, 13.8 million, and 8.2 million. Figure 11 illustrates the maximum stress and deformation of the different components of the three mesh systems. The results indicate a minimal difference in the maximum stress and maximum deformation between the first and second mesh systems. However, the parameters obtained using the third mesh system are significantly different, particularly for the CP component. These discrepancies suggest that the third mesh system is not suitable for accurate mechanical analysis. Considering the impact of the mesh system on the mechanical parameters, a mesh system with 13.8 million meshes is the most appropriate choice for the subsequent mechanics analysis.

Through mesh independence analysis, the optimal mesh size can be determined for both thermal-hydraulics and mechanics calculations, striking a balance between accuracy and computational efficiency. This ensures that the subsequent analyses are performed with a mesh size that provides reliable and consistent results.

Table 4 Nuclear heat deposition before and after structure optimization

Component	Before (MW)	After (MW)	Component	Before (MW)	After (MW)
Breeder 1	0.513	0.377	FW	0.557	0.563
Breeder 2	0.434	0.391	CP 1	0.129	0.029
Breeder 3	0.367	0.370	CP 21	0.100	0.030
Breeder 4	0.331	0.376	CP 22	0.081	0.030
Breeder 5	0.183	0.236	CP 31	0.062	0.030
Multiplier 1	0.217	0.170	CP 32	0.050	0.031
Multiplier 2	0.186	0.174	CP 41	0.035	0.036
Multiplier 3	0.163	0.187	CP 42	0.029	0.036
Multiplier 4	0.141	0.169	CP 51	0.016	0.041
Multiplier 5	0.047	0.069	CP 52	0.011	0.042
W	0.192	0.186	Whole blanket	3.997	3.322

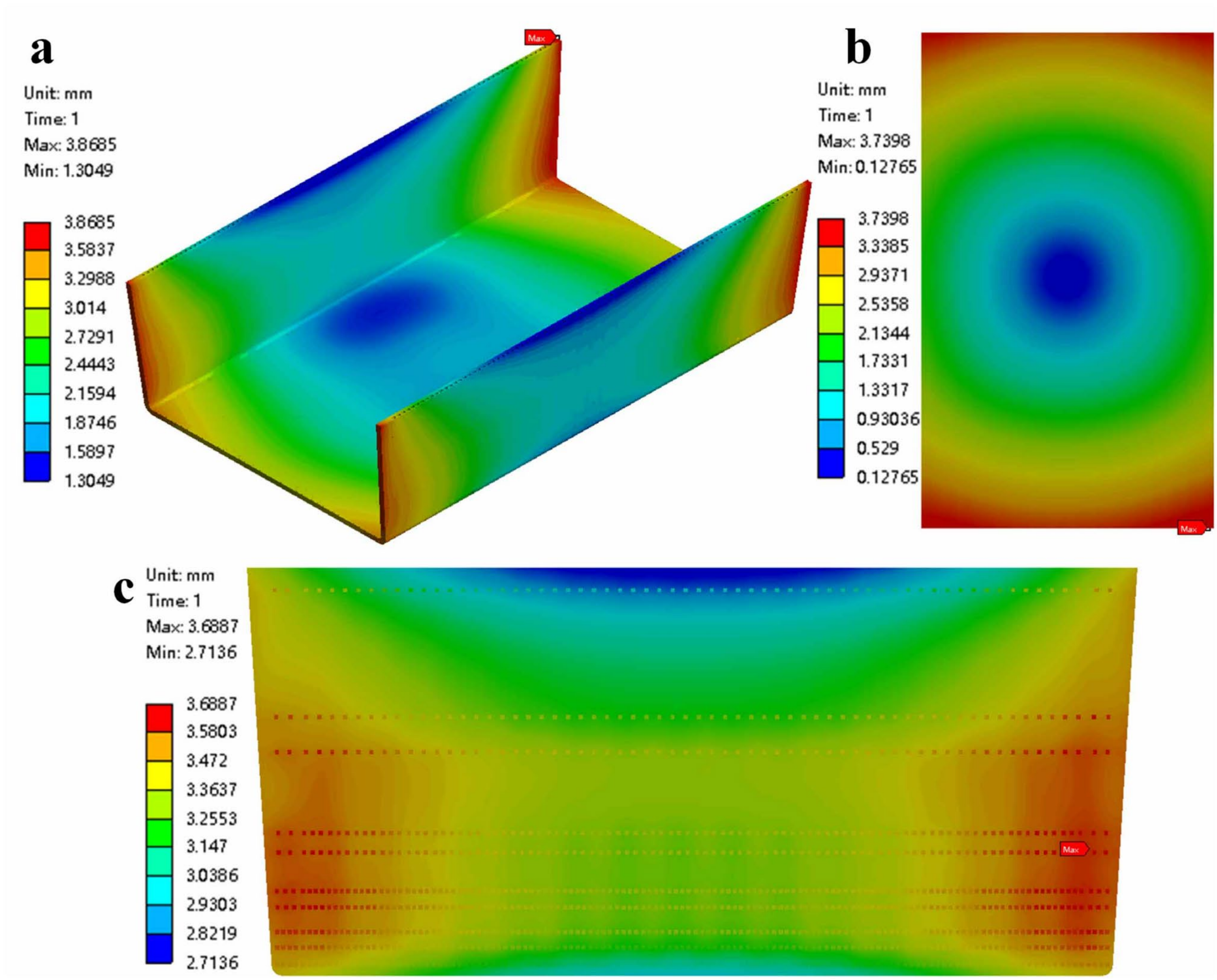

Fig. 13 (Color online) Deformation distribution of typical components after structure optimization: **a** FW; **b** CP32; and **c** Top cap

3.3 Performance analysis

The iterative calculations for the neutronics/thermal-hydraulics coupled analysis revealed that the maximum temperatures of the structural steel, breeder, and multiplier exceeded the temperature limits for the corresponding materials. Specifically, the temperature limits are set to 650, 650, and 900 °C for the ODS RAFM steel, Be, and Li_4SiO_4, respectively. To address this issue, the structure of the CFETR HCCB blanket was optimized [39]. The main modifications involved adjusting the flow channel arrangement and altering the radial thickness of the breeders and multipliers in the function zone. Through a sensitivity analysis, the optimal radial thicknesses are determined and are presented in Table 3. These modifications aim to ensure that the maximum temperatures of these components remain within acceptable limits, thereby enhancing the overall performance and safety of the CFETR HCCB blankets. Figure 12 shows the temperature distribution along the centerline of the blanket after structural optimization. It can be observed that the maximum temperatures in different components of the optimized blanket are all below the temperature limits set for the corresponding materials. The temperature margin for the breeder component is larger than that of the multiplier component. This is primarily because of the higher temperature limit of 900 °C for Li_4SiO_4, which is used as the breeder material. Additionally, the shared cooling system between the breeder and multiplier, separated by the adjacent CP, contributes to a more restricted temperature limit for the multiplier. More detailed descriptions of the thermal-hydraulic parameters before and after structure optimization, based on 3D full-scale blanket models, are reported in [39].

Because of the reduced thickness of most components in the blanket function zone, the overall nuclear heat deposition in the entire blanket diminished, as indicated in Table 4. However, despite the reduction in thickness

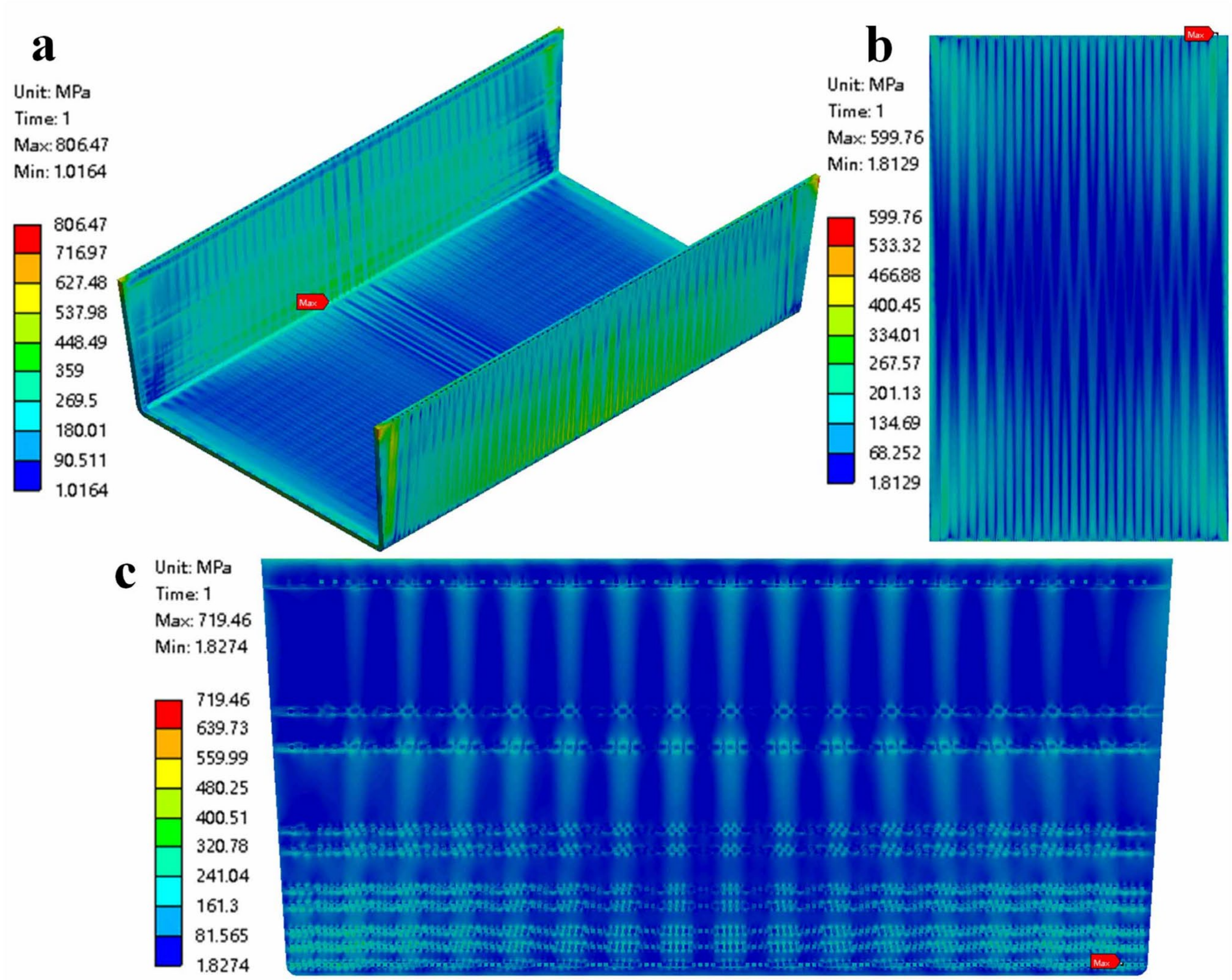

Fig. 14 (Color online) Stress distribution of typical components after structure optimization: **a** FW; **b** CP32; and **c** Top cap

for breeders 1–4 following structural optimization, the nuclear heat depositions in breeders 3 and 4 exhibited a counterintuitive increase. Nuclear heat deposition is influenced by both the neutron flux and nuclear cross-section. In particular, nuclide ^{6}Li in Li_4SiO_4 possesses a larger nuclear cross-section when interacting with thermal neutrons with energies lower than 0.1 MeV. This characteristic led to increased heat deposition in breeders 3 and 4 after structural optimization, although their thicknesses were reduced. This observation highlights the presence of nonlinear feedback within the neutronics/thermal-hydraulics coupling analysis. This demonstrates that changes in geometry and material properties can result in complex interactions and unexpected effects on the nuclear heat deposition distribution within the blanket.

After structural optimization based on the neutronics/thermal-hydraulics coupling analysis, the pressure and temperature data are transferred to the mechanical model of the blanket-supporting structure. Figures 13 and 14 present the mechanical stresses and deformations of typical components. In Fig. 13, the maximum deformation of the different components is approximately 3.75 mm, which is significantly lower than the 20-mm gap between adjacent blankets. This indicates that the deformation of the components remains within an acceptable range. Figure 14 highlights the maximum stress distributions on the FW, CP32, and top caps. In the FW, the maximum stress occurs at the corner because of the large temperature gradient caused by the low cooling capability in this region. This concentrated thermal stress results in a high mechanical stress. Similarly, for CP32, the maximum stress occurs at the joint with the cap, where the flow direction of the coolant changes rapidly, reducing the cooling capability and leading to higher stress levels. With respect to the top cap, the maximum stress is observed at the joint with CP1. In the next section, the stress distribution on various blanket components is linearized for

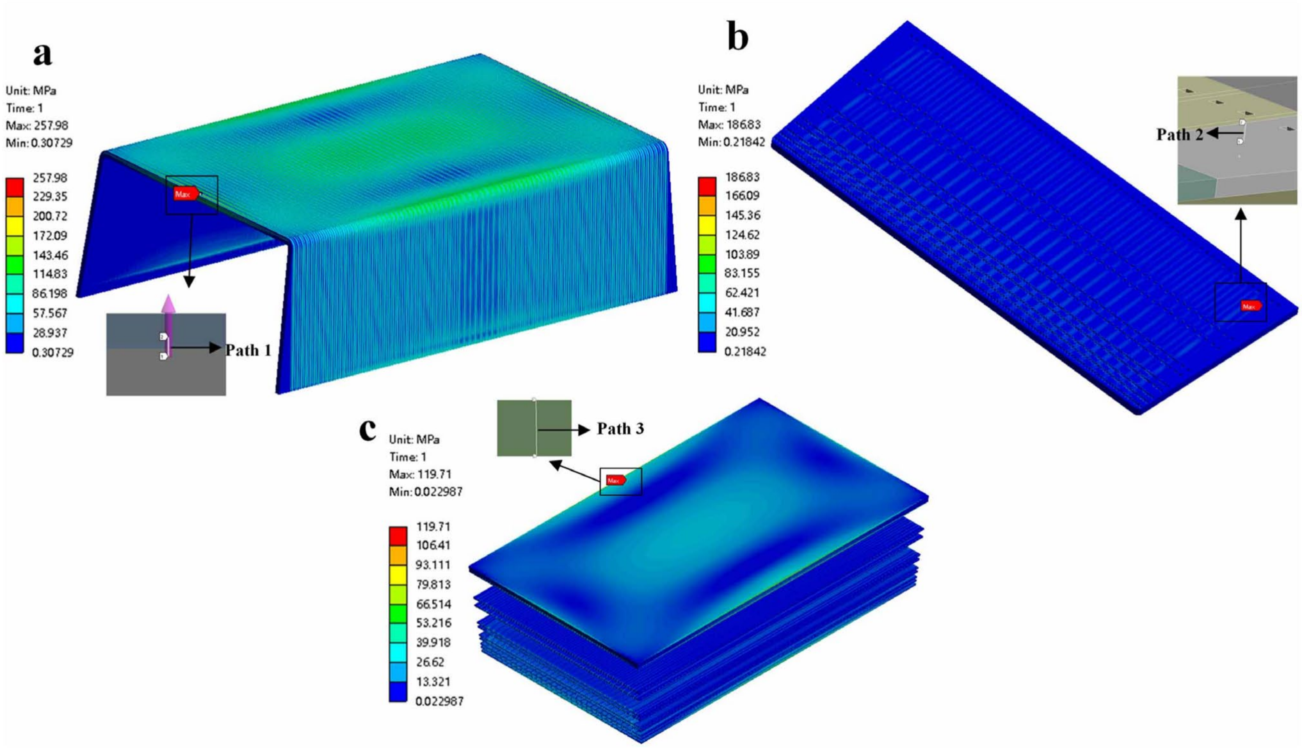

Fig. 15 (Color online) Primary stress distribution on different components: **a** FW; **b** Cap; **c** CP

Table 5 Comparison with design criteria against IPC&IPI

	$\overline{P_m}$			$\overline{P_L + P_b}$		
Location	Value (MPa)	Limit (MPa)	Margin (%)	Value (MPa)	Limit (MPa)	Margin (%)
Path 1	86.5	143.5	+40	147.2	215.5	+32
Path 2	49.6	150.6	+67	113.7	225.9	+50
Path 3	32.8	169.3	+81	53.6	254.0	+79

Table 6 Comparison with design criteria against creep

	$\overline{P_m}$			$\overline{P_L + P_b/1.25}$		
Location	Value (MPa)	Limit (MPa)	Margin (%)	Value (MPa)	Limit (MPa)	Margin (%)
Path 1	86.5	156.8	+45	117.8	156.8	+25
Path 2	49.6	174.6	+72	91.0	174.6	+48
Path 3	32.8	216.0	+85	42.9	216.0	+80

structural assessment according to the structural design criteria SDC-IC [45].

4 Structural assessment of CFETR HCCB blanket

The structural assessment is conducted following a specific procedure. First, the assessment path is determined along the thickness of the component where the equivalent stress is highest. Subsequently, the stress tensor is linearized to obtain the different stress components along this path. The stress components obtained are then compared with the design values to evaluate whether structural integrity could be guaranteed under certain failure modes. The stress components are classified into primary and secondary stresses. The primary stress includes the primary membrane stress P_m, primary bending stress P_b, and additional local membrane stress L_m. The sum of P_m and L_m is referred to as the local membrane stress P_L. By contrast, the secondary stress Q_L mainly refers to the thermal stress induced by the temperature gradient. Structural design criterion SDC-IC [45]

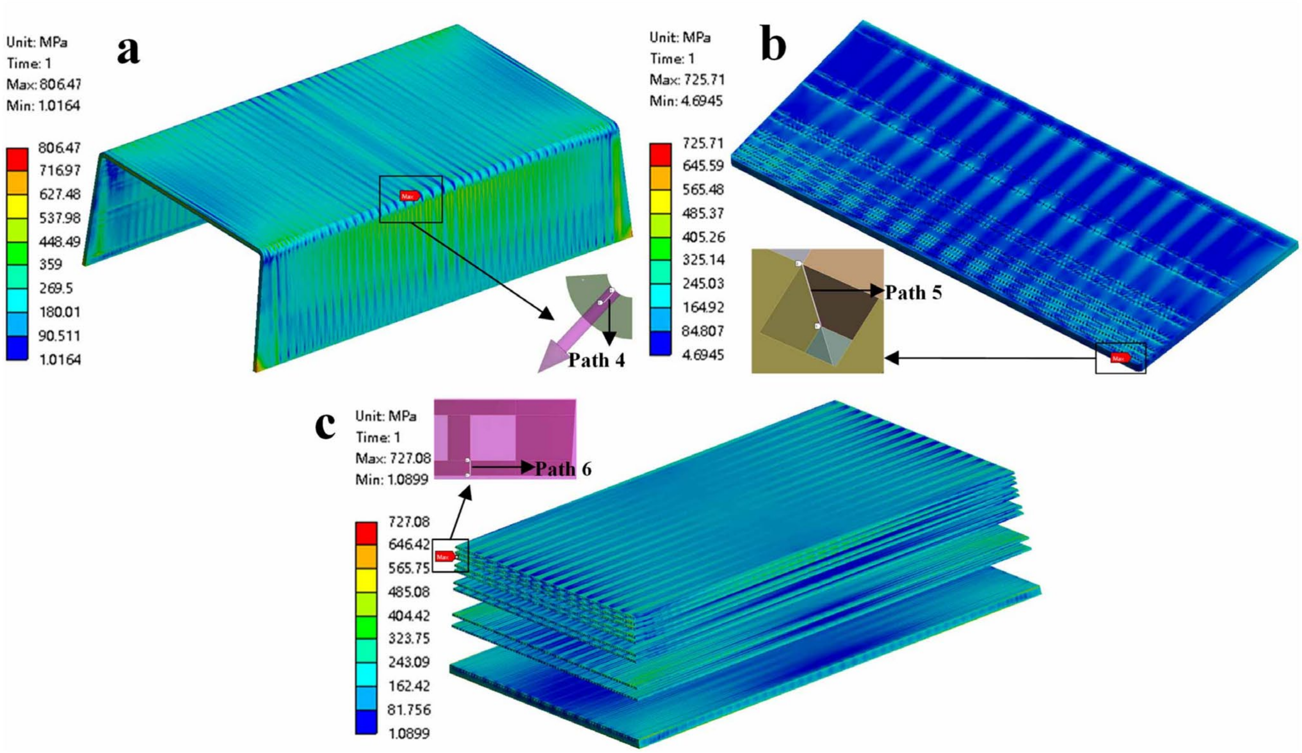

Fig. 16 (Color online) Primary plus secondary stresses distribution on different components: **a** FW; **b** Cap; and **c** CP

Table 7 Comparison with design criteria against ILF and IPFL

	ILF: $\overline{P_L + P_b + Q_L}$			IPFL: $\overline{P_L + Q_L}$		
Location	Value (MPa)	Limit (MPa)	Margin (%)	Value (MPa)	Limit (MPa)	Margin (%)
Path 4	494.5	582.3	+15	206.8	234.2	+12
Path 5	438.6	573.7	+24	253.9	279.4	+9
Path 6	395.2	580.1	+32	237.6	258.7	+8

stipulates the limit values for different stress components under various failure modes. These limitations provide guidelines for evaluating the ability of blanket structures to withstand stress and ensure their integrity.

4.1 Structural assessment under steady state

Under steady-state conditions, the primary stress is assessed for two failure modes: (a) immediate plastic collapse and immediate plastic instability (IPC&IPI) and (b) creep. The primary stress mainly arises from mechanical loading. Figure 15 illustrates the distribution of the primary stress on the different components, considering only the effects of gravity and pressure loading on the blanket. The assessment paths are selected in regions where the equivalent stress is the highest within the structure. Along these assessment paths, stress linearization is performed to determine the values of the different stress components. The obtained stress component values are compared with the design limits specified for each failure mode. Tables 5 and 6 present comparisons of the stress components and corresponding design limits for IPC&IPI and creep failure modes, respectively. Evidently, the margin between the stress components and design limits for all the assessment paths exceeds 25%. This indicates that the CFETR HCCB blanket is designed with a sufficient capability to withstand the two structural failure modes.

Under steady-state conditions, the primary and secondary stresses are assessed for two failure modes: (c) immediate local fracture due to exhaustion of ductility (ILF) and (d) immediate plastic flow localization (IPFL). These failure modes resulted from the combined effects of the primary and secondary stresses induced by mechanical and thermal loading. Figure 16 illustrates the distribution of the primary and secondary stresses on different components, considering the effects of gravity, pressure, and thermal loading on the

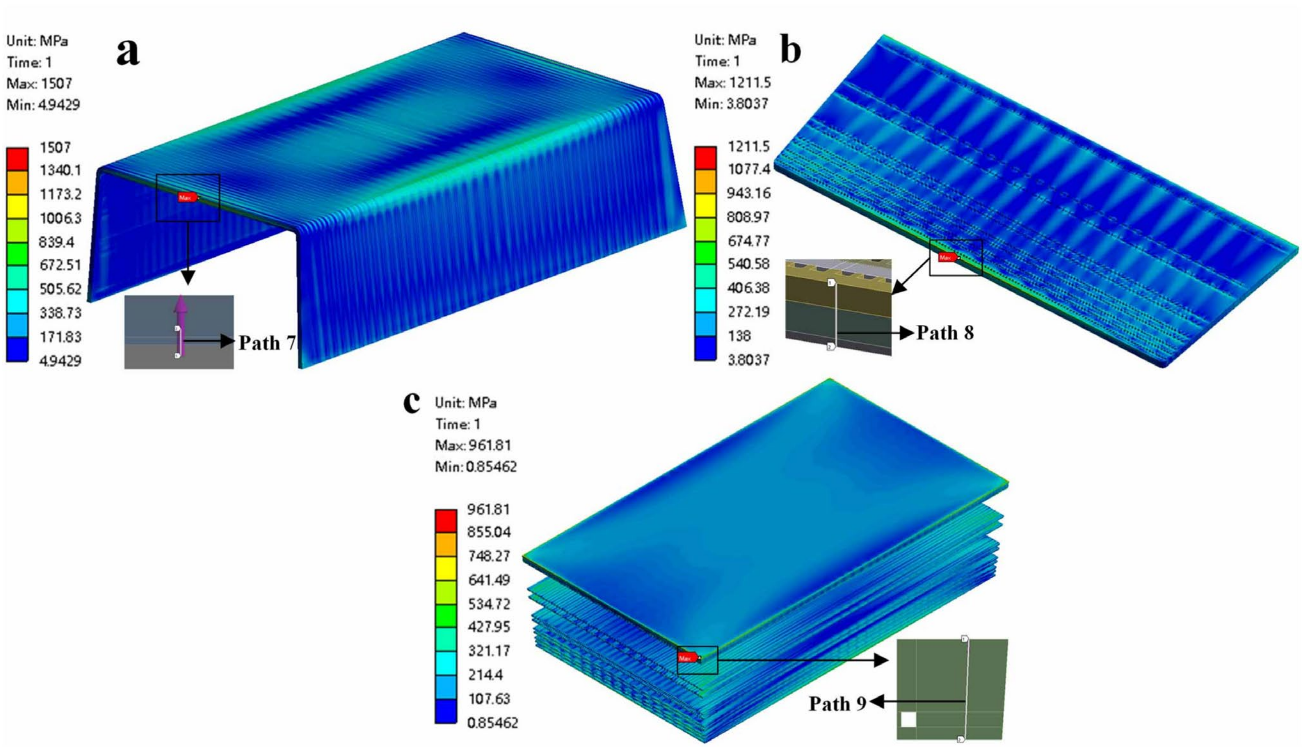

Fig. 17 (Color online) Stress distribution on different components under in-box LOCA: **a** FW; **b** Cap; and **c** CP

Table 8 Comparison with design criteria under in-box LOCA

Location	$\overline{P_m}$			$\overline{P_L + P_b}$		
	Value (MPa)	Limit (MPa)	Margin (%)	Value (MPa)	Limit (MPa)	Margin (%)
Path 7	412.2	309.1	– 33	629.7	463.6	– 35
Path 8	330.1	307.4	– 7	443.8	461.1	– 4
Path 9	323.7	303.5	– 6	334.8	455.2	– 26

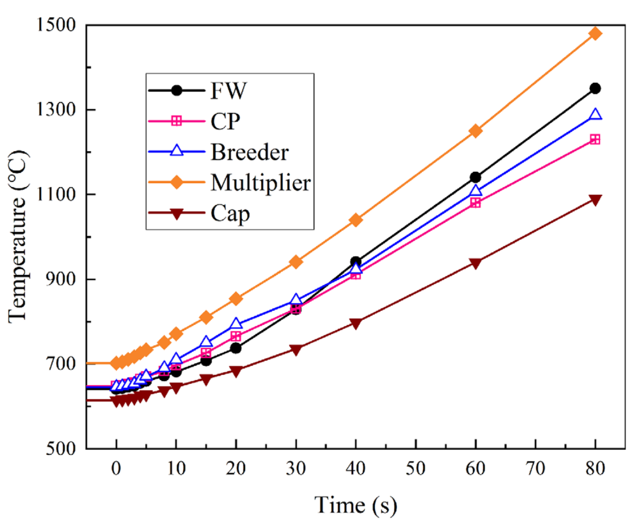

Fig. 18 (Color online) Maximum temperature on different blanket components after LOFA

blanket. The assessment paths are selected in regions where the equivalent stress is the highest within the structure. After stress linearization along these paths, the obtained stress components are compared with the design limits corresponding to each failure mode. Table 7 presents the comparisons of the stress components and corresponding design limits for ILF and IPFL failure modes. It can be observed that the margins for these two failure modes are noticeably lower than those of IPC&IPI and creep, as shown in Tables 5 and 6. This result is primarily due to the significant influence of the secondary stress induced by temperature gradients. Despite this reduced margin, the CFETR HCCB blanket is designed with sufficient capability to withstand all four structural failure modes. This assessment confirms that the blanket exhibits robustness and integrity under steady-state operating conditions, thereby providing confidence in its performance and safety.

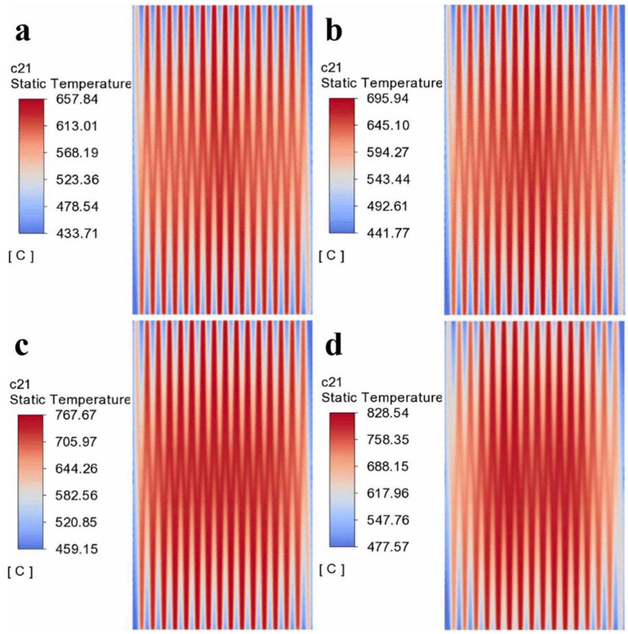

Fig. 19 (Color online) Temperature distribution on CP21 after LOFA: **a** t=3.1 s; **b** t=9.8 s; **c** t=20.2 s; and **d** t=29.7 s

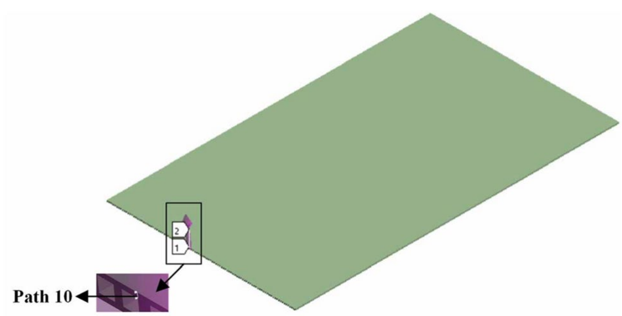

Fig. 20 (Color online) Assessment path on CP21

4.2 Structural assessment under in-box LOCA

According to the structural design criteria SDC-IC [45], the structural assessment for major accidents should follow level D criteria, which mainly focus on the design limit for primary stress. In the in-box LOCA, the high-pressure helium quickly discharges into the blanket box. Therefore, a pressure of 12 MPa is applied to the blanket box in addition to the boundary conditions under steady-state conditions. Figure 17 shows the stress distributions of different components under an in-box LOCA. The highest stress occurs at the joint between the FW and the cap, reaching 1507 MPa. This represents a significant increase compared with the maximum stress of 806 MPa under steady-state conditions, as shown in Fig. 16. The location of the highest stress on the FW is similar to that shown in Fig. 15, indicating that the primary stress is the dominant factor under the in-box LOCA. Table 8 compares the design criteria under the in-box LOCA. The stress components along all the three assessment paths exceeded the design limits, particularly for path 7 on the FW. This result indicates that the blanket skeleton structure fails to meet the design limits, and that the integrity of the blanket may not be maintained under an in-box LOCA. Therefore, further measures should be taken to prevent structural failures. For example, a blanket can be redesigned by adding stiffening plates to enhance its structural strength. Alternatively, pressure-control methods can be implemented to reduce the pressure level in the blanket box. These measures will help ensure the structural integrity and safety of the CFETR HCCB blanket under in-box LOCA conditions.

4.3 Structural assessment under loss-of-flow accident

Under the loss-of-flow accident (LOFA), the flow rate at the blanket inlet rapidly decreases owing to an electrical or mechanical breakdown in the cooling system [46]. In a conservative analysis, the fusion plasma is assumed to operate normally, and no protection method is triggered after the LOFA. The inlet flow rate is obtained from a safety analysis of the LOFA and used as the boundary condition in this study. Figure 18 illustrates the evolution of the maximum temperature for the different components under LOFA. The temperature information of a certain component can be obtained by looping over all the meshes in the component using the compiled UDF. The breeder temperature exceeds the temperature limit of 900 °C for Li_4SiO_4 within 25 s, whereas the multiplier temperature surpasses the temperature limit of 650 °C for Be within 2 s. These two components are not used for the blanket support and are not considered in the structural assessment. For the blanket skeleton structure, the maximum temperature is detected at CP21; this maximum temperature exceeds the temperature limit of 650 °C for the ODS RAFM steel within 2 s. However, this increase in temperature did not immediately cause any structural damage. The temperature distributions at CP21 are shown in Fig. 19 indicates that the maximum temperature is located at the joint between CP21 and the cap. The assessment path is selected based on the location of the maximum temperature as shown in Fig. 20, and stress linearization is performed for the primary stress analysis. On this assessment path, the average primary membrane stress $\overline{P_m}$ is 31.9 MPa, and the average value of $\overline{P_L + P_b}$ is 50.8 MPa. According to the SDC-IC structural design criteria, the temperature corresponding to the design limit for ODS RAFM steel is 719.4 °C. Considering the temperature evolution on CP21 depicted in Fig. 19, the temperature on the assessment path reaches 719.4 °C within 17 s. Therefore, the structural failure of the blanket also occurs within 17 s after LOFA, indicating that the integrity of the blanket is compromised. However, a designed protection method such as turning off the heating power supply is triggered to shut down the plasma if the inlet flow rate decreases to 80% of the normal value [46]. A protection method can be applied within 4 s, even with a signal delay of 3 s. Therefore, an additional 10–15 s available to implement further mitigation methods. Given the overall consideration, the blanket is considered to possess sufficient capability to maintain its structural integrity under LOFA.

5 Conclusion

In this study, a coupling method for neutronics, thermal-hydraulics, and mechanics is developed and applied to a 3D full-scale model of the CFETR HCCB blanket. Through an analysis of neutronics and thermal–hydraulic coupling, the structure of the blanket is optimized to reduce the material temperature. The optimized blanket is then subjected to a structural assessment based on coupling analysis. The main conclusions of this study are summarized as follows:

(1) The UDF code was compiled to facilitate the analysis of neutronics and thermal-hydraulics coupling, whereas the thermal-hydraulics and mechanics coupling analyses were conducted using the Workbench platform. The transfer of data between different calculations was validated, ensuring the preservation of physical conservation during coupling analysis.

(2) During the iterative calculations for neutronics and thermal-hydraulics coupling analysis, all the components of the CFETR HCCB blanket experienced overtemperature issues. Consequently, structural optimization was conducted to mitigate the high material temperatures.

(3) In the steady-state assessment, the CFETR HCCB blanket is designed to have an adequate capability to withstand four structural failure modes: (a) immediate plastic collapse and instability, (b) creep, (c) immediate local fracture due to ductility exhaustion, and (d) immediate plastic flow localization. However, the margin for the fourth failure mode is the lowest owing to the significant impact of the secondary stress induced by the temperature gradients.

(4) In the assessment under an in-box LOCA, the primary stress was found to be the major contributing factor to structural failure. Based on the structural design criteria, all stress components exceeded the designated limits. This indicates that the integrity of the CFETR HCCB blanket may not be maintained during an in-box LOCA.

(5) In the assessment under the LOFA condition, the structural failure of the CFETR HCCB blanket occurred within 17 s in the absence of protective measures. However, the fusion plasma could be shut down within 4 s owing to a decrease in the flow rate. Considering the additional time available for implementing further mitigation methods, we can conclude that the blanket possesses sufficient capability to maintain its structural integrity under an LOFA.

Author Contributions All authors contributed to the study conception and design. Material preparation, data collection, and analysis were performed by Qiang Lian, Kui Zhang, Shan-Shan Bu, Liang-Ming Pan, Wen-Xi Tian, Sui-Zheng Qiu, Guang-Hui Su, Xing-Hua Wu, and Xiao-Yu Wang. The first draft of the manuscript was written by Qiang Lian, and all authors commented on previous versions of the manuscript. All authors read and approved the final manuscript.

Data Availability The data that support the findings of this study are openly available in Science Data Bank at https://cstr.cn/31253.11.sciencedb.j00186.00965 and https://www.doi.org/10.57760/sciencedb.j00186.00965.

Declarations

Conflict of interest The authors declare that they have no conflict of interest.

References

1. M. Abdou, N.B. Morley, S. Smolentsev et al., Blanket/first wall challenges and required R&D on the pathway to DEMO. Fusion Eng. Des. **100**, 2–43 (2015). https://doi.org/10.1016/j.fusengdes.2015.07.021
2. H.M. Sahin, G. Tunç, A. Karakoç et al., Neutronic study on the effect of first wall material thickness on tritium production and material damage in a fusion reactor. Nucl. Sci. Tech. **33**, 43 (2022). https://doi.org/10.1007/s41365-022-01029-7
3. H.X. Wang, X.W. Fu, W.P. Liu et al., Numerical simulation of tritium behavior under a postulated accident condition for CFETR TEP system. Nucl. Sci. Tech. **34**, 109 (2023). https://doi.org/10.1007/s41365-023-01260-w
4. J.H. Jiang, X.W. Cao, Simulation study of tritium atmospheric dispersion of loss of vacuum accident of a fusion reactor. Nucl. Tech. (in Chinese) **46**, 020605 (2023). https://doi.org/10.11889/j.0253-3219.2023.hjs.46.020605
5. Z.K. Zeng, S.Z. Chen, Y. Zhang et al., Neutronics experiments of dual functional lithium-lead blanket based on D-T fusion neutron source. Nucl. Tech. (in Chinese) **45**, 040601 (2022). https://doi.org/10.11889/j.0253-3219.2022.hjs.45.040601
6. G.C. Zhang, J. Liu, L.Z. Cao et al., Neutronic calculations of the China dual-functional lithium-lead test blanket module with the parallel discrete ordinates code Hydra. Nucl. Sci. Tech. **31**, 8 (2020). https://doi.org/10.1007/s41365-020-00789-4
7. H.D. Luo, Y. Lin, B. Li et al., Comparison of CFETR nuclear fusion power plant thermal storage technology. Nucl. Tech. (in

Chinese) **47**, 050014 (2024). https://doi.org/10.11889/j.0253-3219.2024.hjs.47.050014
8. B.W. Zheng, C.Y. Jiang, Z.H. Liu et al., Correction and verification of HL-2A Tokamak Bonner sphere spectrometer in monoenergetic neutron fields from 100 keV to 5 MeV. Nucl. Sci. Tech. **30**, 159 (2019). https://doi.org/10.1007/s41365-019-0689-9
9. R. Che, S.C. Liu, Z. Tian et al., Shielding calculation based on SINBAD fusion benchmarks using cosRMC. Nucl. Tech. (in Chinese) **47**, 050008 (2024). https://doi.org/10.11889/j.0253-3219.2024.hjs.47.050008
10. Y.Q. Chen, J. Wang, B. Wu et al., Activation and shutdown doserate analyses for the EAST NBI test facility. Nucl. Sci. Tech. **27**, 85 (2016). https://doi.org/10.1007/s41365-016-0079-5
11. W.K. Chen, L.Q. Hu, G.Q. Zhong et al., Optimization study and design of scintillating fiber detector for D-T neutron measurements on EAST with Geant4. Nucl. Sci. Tech. **33**, 139 (2022). https://doi.org/10.1007/s41365-022-01123-w
12. Q. Sheng, S.Q. Wu, X.Y. Wang et al., Overview of the ITER TBM program. Nucl. Tech. (in Chinese) **45**, 070001 (2022). https://doi.org/10.11889/j.0253-3219.2022.hjs.45.070001
13. S.Z. Wang, S.C. Liu, Y.X. Chen, Transport-activation internal coupling method for fusion reactors based on cosRMC. Nucl. Tech. (in Chinese) **47**, 050007 (2024). https://doi.org/10.11889/j.0253-3219.2024.hjs.47.050007
14. D.L. Zhang, S.J. Cui, J. Cheng et al., Improving the optimization algorithm of NTCOC for application in the HCSB blanket for CFETR Phase II. Fusion Eng. Des. **135**, 216–227 (2018). https://doi.org/10.1016/j.fusengdes.2018.07.027
15. S. Qu, Q.X. Cao, X.R. Duan et al., Study on multiphysics coupling and automatic neutronic optimization for solid tritium breeding blanket of fusion reactor. Energies **14**, 5442 (2021). https://doi.org/10.3390/en14175442
16. Q. Lian, W.X. Tian, S.Z. Qiu et al., Neutronics influence of poloidal nonuniform neutron wall loading on helium-cooled ceramic breeder blanket for CFETR. Fusion Eng. Des. **161**, 111950 (2020). https://doi.org/10.1016/j.fusengdes.2020.111950
17. Q.X. Cao, X.Y. Wang, X.H. Wu et al., Neutronics and shielding design of CFETR HCCB blanket. Fusion Eng. Des. **172**, 112918 (2021). https://doi.org/10.1016/j.fusengdes.2021.112918
18. Q. Lian, S.M. Tang, L.X. Zhu et al., Three-dimensional thermal-hydraulics/neutronics coupling analysis on the full-scale module of helium-cooled tritium-breeding blanket. Nucl. Eng. Technol. **55**, 4274–4281 (2023). https://doi.org/10.1016/j.net.2023.08.005
19. B. Zhou, B. Hu, Y.L. Wang et al., Preliminary accident analyses of in-box LOCA for CFETR HCCB blanket system. Fusion Eng. Des. **196**, 114005 (2023). https://doi.org/10.1016/j.fusengdes.2023.114005
20. X.Y. Wang, K.M. Feng, Y.J. Chen et al., Current design and R&D progress of the Chinese helium cooled ceramic breeder test blanket system. Nucl. Fusion **59**, 076019 (2019). https://doi.org/10.1088/1741-4326/ab0c32
21. G. Zhuang, G.Q. Li, J. Li et al., Progress of the CFETR design. Nucl. Fusion **59**, 112010 (2019). https://doi.org/10.1088/1741-4326/ab0e27
22. K.F. Zhang, S. Wang, H.L. Chen, Electromagnetic-thermal two-way coupling analysis and application on helium-cooled solid blanket. Nucl. Eng. Technol. **55**, 927–938 (2023). https://doi.org/10.1016/j.net.2022.11.005
23. Q.Q. Xu, S. Wang, H.L. Chen et al., Comprehensive analysis of electromagnetic and thermal-mechanical effects on HCSB under MD event for CFETR. Fusion Eng. Des. **138**, 294–302 (2019). https://doi.org/10.1016/j.fusengdes.2018.11.043
24. K. Pei, M.X. Lu, Study on the effect of poloidal segmentation of breeder blanket of CFETR on the electromagnetic load distribution. Nucl. Tech. (in Chinese) **43**, 010601 (2020). https://doi.org/10.11889/j.0253-3219.2020.hjs.43.010601
25. M. Wang, M.Z. Lei, Y.T. Song et al., Electromagnetic-structural coupling analysis on CFETR helium cold ceramic breeder blanket under plasma major disruption. Nucl. Tech. (in Chinese) **40**, 060601 (2017). https://doi.org/10.11889/j.0253-3219.2017.hjs.40.060601
26. S.J. Cui, D.L. Zhang, J. Cheng et al., Numerical research on the neutronic/thermal-hydraulic/mechanical coupling characteristics of the optimized helium cooled solid breeder blanket for CFETR. Fusion Eng. Des. **114**, 141–156 (2017). https://doi.org/10.1016/j.fusengdes.2016.12.013
27. K.C. Jiang, W.Q. Ding, X.K. Zhang et al., Development of neutronic-thermal hydraulic-mechanic-coupled platform for WCCB blanket design for CFETR. Fusion Eng. Des. **137**, 312–324 (2018). https://doi.org/10.1016/j.fusengdes.2018.10.013
28. K.C. Jiang, X.K. Zhang, J. Li et al., Using one hybrid 3D–1D-3D approach for the conceptual design of WCCB blanket for CFETR. Fusion Eng. Des. **114**, 57–71 (2017). https://doi.org/10.1016/j.fusengdes.2016.12.002
29. J. Cheng, Y.W. Wu, S.J. Cui et al., Conceptual design and coupled neutronic/thermal-hydraulic/mechanical research of the supercritical water cooled ceramic blanket for CFETR. Fusion Eng. Des. **138**, 272–281 (2019). https://doi.org/10.1016/j.fusengdes.2018.11.042
30. G.M. Zhou, F. Hernandez, L.V. Boccaccini et al., Preliminary structural analysis of the new HCPB blanket for EU DEMO reactor. Int. J. Hydrogen Energ. **42**, 7053–7058 (2016). https://doi.org/10.1016/j.ijhydene.2016.01.064
31. I. Catanzaro, G. Bongiovi, P.A. Di Maio et al., Structural assessment of the EU-DEMO water-cooled lead lithium central outboard blanket segment adopting the sub-modelling technique. Fusion Eng. Des. **192**, 113601 (2023). https://doi.org/10.1016/j.fusengdes.2023.113601
32. S.J. Cui, Y.H. Lang, Q. Lian et al., Neurtonics/Thermal-hydraulic analyses of the CFETR HCCB blanket for multiple operation modes under the poloidal nonuniform neutron wall loading condition. Fusion Eng. Des. **168**, 112612 (2021). https://doi.org/10.1016/j.fusengdes.2021.112612
33. M.Y. Zheng, W.X. Tian, H.Y. Wei et al., Development of a MCNP-ORIGEN burn-up calculation code system and its accuracy assessment. Ann. Nucl. Energy **63**, 491–498 (2013). https://doi.org/10.1016/j.anucene.2013.08.020
34. B. Zhou, H. Zhang, Y. Ji et al., Numerical investigation on turbulent flow and heat transfer of helium-xenon gas mixture in a circular tube. Sci. Technol. Nucl. Ins. **2021**, 8356893 (2021). https://doi.org/10.1155/2021/8356893
35. Q.W. Liu, M. Li, S. Wang et al., Thermal-mechanical analysis of the first wall for CFETR helium cooled solid breeder blanket. Ann. Nucl. Energy **85**, 12–16 (2015). https://doi.org/10.1016/j.anucene.2015.04.030
36. L.R. Ye, M.J. Wang, X.A. Wang et al., Thermal hydraulic and neutronics coupling analysis for plate type fuel in nuclear reactor core. Sci. Technol. Nucl. Ins. **2020**, 2562747 (2020). https://doi.org/10.1155/2020/2562747
37. S.J. Cui, D.L. Zhang, Q. Lian et al., Development of a neutronics/thermal-hydraulic coupling optimization code and its application on the CFETR HCSB blanket. Fusion Eng. Des. **122**, 140–153 (2017). https://doi.org/10.1016/j.fusengdes.2017.08.023
38. J. Reimann, S. Hermsmeyer, Thermal conductivity of compressed ceramic breeder pebble beds. Fusion Eng. Des. **61**, 345–351 (2002). https://doi.org/10.1016/S0920-3796(02)00165-5
39. Q. Lian, S.M. Tang, L.X. Zhu et al., Structure optimization of helium-cooled blanket for fusion reactor based on three-dimensional full-scale thermal-hydraulic analysis. Fusion Eng. Des. **194**, 113922 (2023). https://doi.org/10.1016/j.fusengdes.2023.113922
40. S.L. Liu, X.M. Cheng, X.B. Ma et al., Progress on design and related R&D activities for the water-cooled breeder blanket for

CFETR. Theor. Appl. Mech. Lett. **9**, 161–172 (2019). https://doi.org/10.1016/j.taml.2019.03.001
41. Y.T. Luo, H. Du, Y.M. Yan, MeshCNN-based BREP to CSG conversion algorithm for 3D CAD models and its application. Nucl. Sci. Tech. **33**, 74 (2022). https://doi.org/10.1007/s41365-022-01063-5
42. D. Große, U. Fischer, K. Kondo et al., Status of the McCad geometry conversion tool and related visualization capabilities for 3D fusion neutronics calculations. Fusion Eng. Des. **88**, 2210–2214 (2013). https://doi.org/10.1016/j.fusengdes.2013.02.146
43. X.C. Nie, J. Li, S.L. Liu et al., Global variance reduction method for global Monte Carlo particle transport simulations of CFETR. Nucl. Sci. Tech. **28**, 115 (2017). https://doi.org/10.1007/s41365-017-0270-3
44. Y.F. Qiu, P. Lu, U. Fischer et al., A generic data translation scheme for the coupling of high-fidelity fusion neutronics and CFD calculations. Fusion Eng. Des. **89**, 1330–1335 (2014). https://doi.org/10.1016/j.fusengdes.2014.02.044
45. S. Sadakov, S. Khomiakov, B. Calcagno et al., Status of ITER blanket attachment design and related R&D. Fusion Eng. Des. **88**, 1853–1857 (2013). https://doi.org/10.1016/j.fusengdes.2013.03.031
46. Q. Lian, W.X. Tian, S.J. Cui et al., Preliminary safety assessment on two LOCAs under ITER-like condition for the optimized CFETR helium cooled solid breeder blanket. Fusion Eng. Des. **121**, 235–244 (2017). https://doi.org/10.1016/j.fusengdes.2017.07.018